A COMPREHENSIVE STUDY ON MICROSTRUCTURE AND MECHANICAL PROPERTIES OF SLM PRINTED F357 ALLOY FOR VARIOUS PROCESS PARAMETERS

[1a]Ranjith Kumar G S, [1b] Suhas H Nayak, [1c]Shiv Pratap Singh Yadav, [1d]Vijay Kumar S, [1e]Kiran Aithal S, [1f]Nithin U Aithal

1[a, b, c, d, e, f], Department of Mechanical Engineering, Nitte Meenakshi Institute of Technology, Bangalore, India-560064.

[a]24739.ranjith@nmit.ac.in; [b]24671.suhas@nmit.ac.in; [c]vijaysnitk@gmail.com; - [d]shivpratapsinghyadav@nmit.ac.in; [e]kiranaithal.s@nmit.ac.in; [f]nithin.ua@nmit.ac.in

Abstract: The usage of aluminium (Al) metal components made using selective laser melting (SLM) and additive manufacturing (AM) (SLM). As a result, new high strength aluminium alloys have been developed that are more suited to the additive manufacturing (AM) process parameters, such as power (w), scan speed (m/s), and hatch distance (Hd). This study examines and contrasts the microstructure, which is crucial in determining the characteristics. Through the use of vertically and horizontally constructed specimens made of Alsi10Mg and the laser beam powder bed fusion (LB-PBF) Am method, various Al alloys' porosity and fatigue behaviours were created. Process parameters are established by a test campaign to ensure a density of at least 95%. Based on these findings, samples are then created for microstructural and mechanical evaluation, with laser power ranging from 100W to 150W and hatch distance starting at 0.08. mm to 0.12 mm with a 90° orientation. All experiments are conducted on an SLM machine with a laser output of up to 150W and a spot diameter of 50 m. Following the examinations, some intriguing information regarding the variations for the alloys was discovered.

Keywords: Aluninum (Al); Density LB-PBF; SLM; AM; Microstructure;

1. INTRODUCTION

The layer-by-layer addition of material in the additive manufacturing (AM) process, coupled with the quick pace of part creation, has revolutionized a variety of sectors and offers significant advantages in some applications [1]. The feedstock material is often melted in metal-based AM using an electron or laser source. Laser-engineered net shaping, electron beam melting, and selective laser melting are a few of the procedures (LENS) [2]. Laser-based powder fusion (L-PBF).A wide range of metallic materials, including steel, titanium, nickel, and alloys of aluminium, are processed. Due to their comparatively low cost, light weight, and great strength, aluminium alloys are particularly intriguing for a variety of applications [3].

Traditional cast Al-Si-Mg alloys are the most popular and researched among aluminium alloys due to their excellent laser process ability regarding the L-PBF method [4]. Due to both its almost composition, which provides a small range of solidification and high Si content, which ensures a good degree of fluidity when it's molten, the specific AlSi7NMg has by far drawn the most interest.

These L-PBF process components are crucial because they enable the creation of completely dense and crack-free products. The modern era of welding is just getting started, and it's getting inventors thinking about the finest methods to combine metals [5]. Due to the extensive use of rivets, screws, and bolts to join metals, this is the beginning of the end.

2. METHODOLOGY

2.1 Hardness Test:

29 days after the samples were cast, measurements of hardness were made. The conclusions are illustrated using analyses of the graphite mould and the croning cell for the alloys AlSi7Mg and AlSi7MgLi. It is clear that the Li addition significantly affects the alloy's hardness [6]. With a slower cooling rate of 5 K/s between HV 63 and 71 and an up to 36 percent faster cooling rate (160 K/s), between 69 and 95 HV, the unique AlSi7MgLi alloy has a tougher first day after casting than the ordinary alloy [7]. It is evident that the enhanced hardness is due to the Li addition process for strengthening solutions, which results in an Al replacement solid solution [8]. What constitutes the fundamental solid and phase in the microstructure contribute to this increase in difficulty. At quicker cooling rates than slower cooling rates, the hardness increases by around three times as a result of the finer, more saturated solid solution-evenly dispersed microstructural components (SDAS) [9].

Figure 1: Hardness Tester [10].

3. RESULTS AND DISCUSSIONS

3.1 Hardness Test

Table 1: Hardness Test Results

Sl/No	Sample No	P (W)	SS (mm/s)	D_h (mm)	Hardness (VHN)
1	Sample 1	100	200	0.05	201.20
2	Sample 2	100	300	0.07	199.80
3	Sample 3	100	400	0.09	198.52
4	Sample 4	150	200	0.07	198.65
5	Sample 5	150	300	0.09	197.89
6	Sample 6	150	400	0.05	196.55
7	Sample 7	200	200	0.09	197.44
8	Sample 8	200	300	0.05	196.50
9	Sample 9	200	400	0.07	196.41

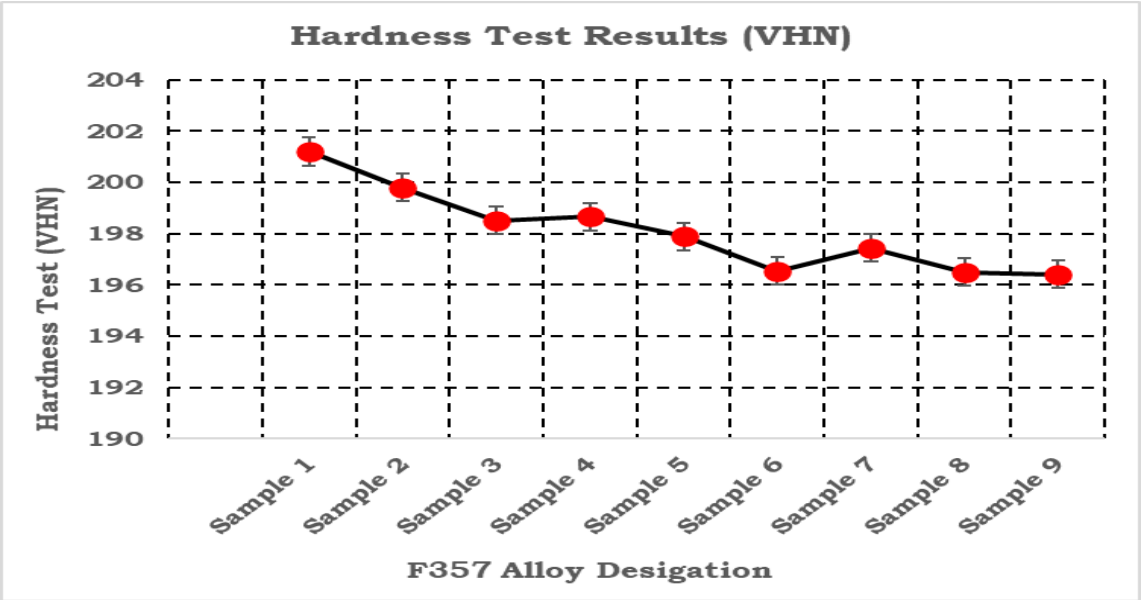

Figure 2: Hardness Test Results of AlSi7Mg

Table 1 displays the constituent properties of the AlSi7Mg alloy. As shown in table 1, with input power of 100W, scan speed of 200(mm/s), and hatch distance of 0.05mm, the output density for sample 1 is reached at 201.20(VHN). The power injection rate is the same for sample 2 as well. 100W of power, 400(mm/s) of scan speed, and a hatch are the inputs for Sample 3. At 100W, 300(mm/s) of scan speed, and 0.07mm of hatch distance, the output density is obtained, which is 199.80. (VHN) [11]. The output density at a distance of 0.09 mm is 198.52. (VHN) The parameters power at 150W, scan speed at 200(mm/s), and hatch distance at 0.07mm are the inputs for sample 4, which produces the output density. And is 198.65 (VHN) The inputs are for sample 5, and they are a hatch, 150W of power, and a 300mm/s scan speed. At a distance of 0.09 mm, the output density is 197.89. (VHN) The inputs are for sample 6, and a 150W power, a 400(mm/s) scan speed, and 0.05mm hatch spacing are used to determine the output density. 196.55(VHN). The inputs for sample 7 include a hatch, a 200W power source, and a 200(mm/s) scan speed. The output density is calculated to be 197.44 at a distance of 0.09mm (VHN) [12]. Using a power of 200W, a scan speed of 300(mm/s), and a hatch distance of 0.05mm, sample 8's inputs yield an output density of 196.50. And is 198.6 (VHN) The inputs for sample 9 are 200W of power and 400(mm/s) of scan speed, and the output density, which is discovered at a distance of 0.07 mm and is 196.41, is found at these inputs (VHN).

3.2 Experimental and Predicted Values of Hardness Test

Table 2: Experimental and Predicted Valves Hardness Test (AlSi7Mg)

Experimental	Predicted	Residual
201.20	200.584	0.616111
199.50	199.551	-0.050556
198.52	198.517	0.002778
198.64	199.039	-0.398889
197.89	198.006	-0.115556
196.55	197.172	-0.622222
197.44	197.494	-0.053889
196.50	196.661	-0.160556
196.41	195.627	0.782778

Table 2 displays the experimental and projected outcomes of the AlSi7Mg density test results. The sample 3 result, where the experimental result is 198.52 and the forecasted value is 198.517, generates the most accurate result, according to the table. The least significant number is 0.002778. The largest inaccuracy in the sample is in comparison, the observed result (196.41) and the anticipated value in Example 6 diverge by 0.782778. (195.627).

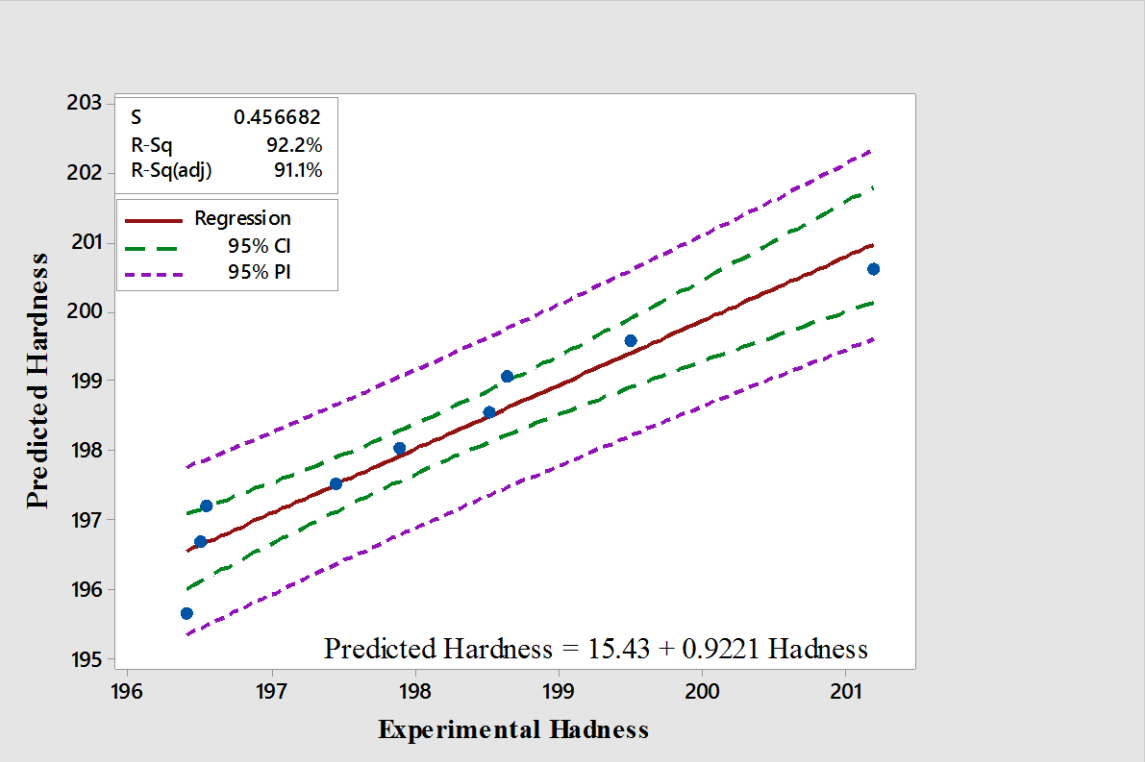

Figure 3: Predicted Hardness Valves of AlSi7Mg

Figure 3 shows a graph showing all AlSi7Mg samples' expected and actual hardness values. In this illustration, the green dotted lines denote experimental hardness values whereas the purple dotted lines reflect predicted hardness values [13]. We can only see three examples in this case that deviate from the experimental hardness line, although there are nearly three more samples with higher inaccuracy than the others.

3.4 Regression Analysis of Hardness Valves of Alsi7Mg

A series to determine the correlations between a dependent variable and one or more independent variables, statistical methods referred to as regression analysis are used [14]. It is applicable to forecast future interactions between variables and evaluate how strong such correlations are right now.

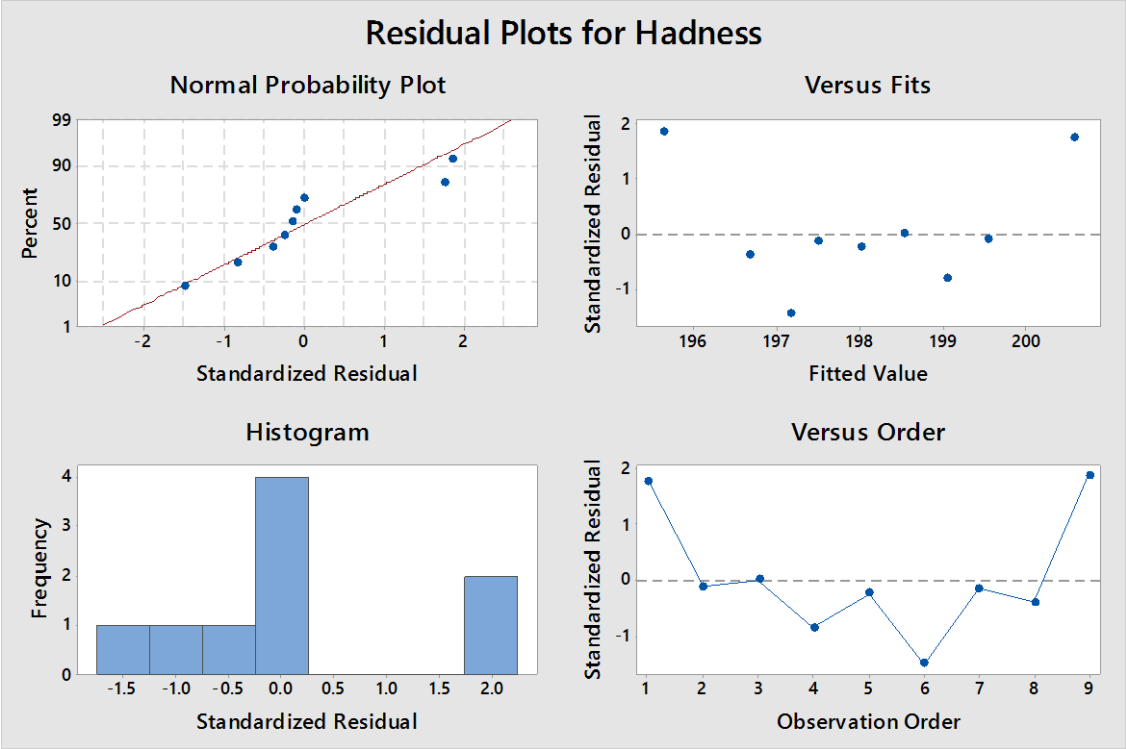

Figure 4: Residual Plots for Hardness Valves for all Combinations Considered

Figure 4: One instance for all combinations, different graphs and statistical charts can be produced using probability and residual density plots [15]. The normalized residual is shown in the normal probability plot along with a percentage. As fitted value vs standardized residual, fits versus fits can be stated [16]. A histogram can be expressed using frequency versus normalized residual. Observation order vs. standardized residual can be used to represent the reverse order.

4. CONCLUSION

The construction parameters used in this study to create fully dense F357 samples by the L - PBF can easily process the F357 powder. P = 100 W, v =700 mm/s, and hd = 0.12mm were the optimal parameters for creating F357 fully dense samples. In comparison to the as-built condition, The hardness of the F357 sample increased upon direct ageing. The greatest hardness value, 146 5 HV, was obtained after a 6-hour 170 C heat treatment for DA. due to the alloying's disintegration components and the following ageing The S-SHT sample obtained the lowest hardness value after heat treatment at 170 C. This led the hardness to increase to 132 3 HV.These findings suggest that the suggested brief L-PBF F357 sample T6 heat treatment is promising. According to the mechanical and microstructural analyses, the 15-minute heating of a solution is faster than the standard SHT, which takes around 8 hours to achieve a solid solution that is supersaturated. The hardness value increases as a result of the subsequent T6 treatment. Because it would mean less post processing time and expense for AM products, the usage of this heat treatment might be very advantageous for the manufacturing line. According to the results of the tensile testing. the DA-6 sample exhibited a lower elongation at break than the AB sample but had the greatest YS with a value of 268 MPa. The S-T6-6 treatment showed considerably larger elongation at break than the other two treatments despite having a somewhat lower YS and UTS.

Reference

1. Dipl. Eng. Bojanova N Institute of Metal Science, Equipment and Technologies with Centre for Hydro and Aerodynamics Introduction OF AlSi7Mg
2. Min Wang, M., Zhang, Y., Song, B. et al. (2018) "Wear Performance and Corrosion Behavior of Nano-SiCp-Reinforced AlSi7Mg Composite" 1212:2,123-122 https://doi.org/10.1007/s40195-021-01220-6
3. Bo Song, B., Zhao, X., Li, S. et al. 2015 "Differences in microstructure and properties Between selective laser melting and traditional manufacturing for fabrication of metal Parts" pg111–125 https://doi.org/10.1007/s11465-015-0341-2
4. 4.Wang Jing 2008 "Formation and evolution of non-dendrite microstructure of Al-Si alloy"
5. Liangju He November 2011 "Microstructure of asymmetric twin roll cast Alsi7Mg magnesium alloy" Pg.2372-2377
6. Simone Romano 2019 "Thermo-mechanical Fatigue Behaviour of AlSi7Mg Processed by Selective Laser Melting" pg1343-1545
7. M. Bayhan 30 August 2021 "PBF Based AlSi7Mg Parts for Aerospace Applications" https://doi.org/10.1007/s12633-021-01474-w
8. Pavel Kasyanov, November 29, 2013 "Investigation of the Mechanical properties of castings of Alloy Alsi7Mg" pg.1242-1453 https://doi.org/10.1177/1740349913510295
9. A.K. Srivastava, M. Maurya, A. Saxena, N.K. Maurya, S.P. Dwivedi, A.R analysis of A359/Si3N4 surface composite produced by friction stir processing Int J Mater Res, 112 (1) (2021), pp. 68-77, 10.1515/ijmr-2020-78277753
10. YongyueLiu[abc]JingkunLi[a] September–October2021 Improving ductility of AlSi7Mg alloy by casting-forging process: of deformation degree Pages 2571-2578 https://doi.org/10.1016/j.jmrt.2021.07.162
11. M. Aamir, K. Giasin, M. Tolouei-Rad, A. Vafadar A review: drilling performance and hole quality of aluminium alloys for aerospace applications J Mater Res Technol, 9 (6) (2020), pp. 12484-12500, 10.1016/j.jmrt.2020.09.003
12. R. Arrabal, B. Mingo, A. Pardo, M. Mohedano, E. Matykina, I. Rodríguez Pitting corrosion of rheocast A356 aluminium alloy in 3.5 wt.% NaCl solution Corros Sci, 73 (2013), pp. 342-355, 10.1016/j.corsci.2013.04.023
13. M. Aamir, K. Giasin, M. Tolouei-Rad, A. Vafadar **A review: drilling performance and hole quality of aluminium alloys for aerospace applications**J Mater Res Technol, 9 (6) (2020), pp. 12484-12500, 10.1016/j.jmrt.2020.09.003
14. M. Wang, B. Song, Q. Wei, Y. Zhang, Y. Shi Effects of annealing on the microstructure and mechanical properties of selective laser melted AlSi7Mg alloy Mater Sci Eng, A, 739 (2019), pp. 463-472, 10.1016/j.msea.2018.10.047
15. I. Öztürk, G.H. Ağaoğlu, E. Erzi, D. Dispinar, G. Orhan Effects of strontium addition on the microstructure and corrosion behavior of A356 aluminum alloyJ Alloys Compd, 763 (2018), pp. 384-391, 10.1016/j.jallcom.2018.05.341
16. M. Cardinale, D. Maccio, G. Luciano, E. Canepa, P. Traverso Thermal and corrosion behavior of as cast AlSi alloys with rare earth elements J Alloys Compd, 695 (2017), pp. 2180-2189, 10.1016/j.jallcom.2016.11.066